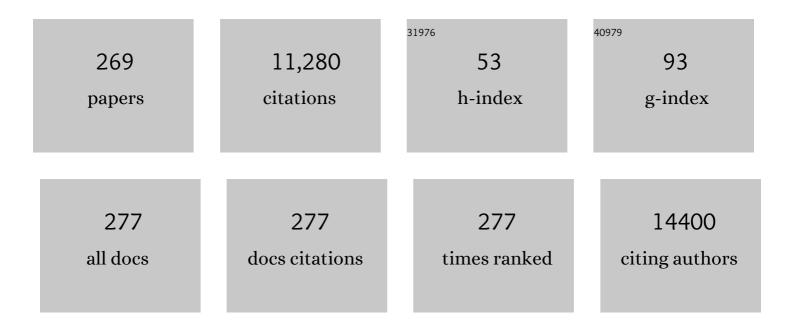
List of Publications by Year in descending order

Source: https://exaly.com/author-pdf/31327/publications.pdf Version: 2024-02-01



HUAN WANC

#	Article	IF	CITATIONS
1	Dual Signals Electrochemical Biosensor for Pointâ€ofâ€Care Testing of Amino Acids Enantiomers. Electroanalysis, 2022, 34, 316-325.	2.9	5
2	Diurnal mood variation symptoms in major depressive disorder associated with evening chronotype: Evidence from a neuroimaging study. Journal of Affective Disorders, 2022, 298, 151-159.	4.1	6
3	Disrupted fronto-parietal network and default-mode network gamma interactions distinguishing suicidal ideation and suicide attempt in depression. Progress in Neuro-Psychopharmacology and Biological Psychiatry, 2022, 113, 110475.	4.8	13
4	Nanomotorâ€Đerived Porous Biomedical Particles from Droplet Microfluidics. Advanced Science, 2022, 9, e2104272.	11.2	31
5	Multiple Stimuliâ€Responsive MXeneâ€Based Hydrogel as Intelligent Drug Delivery Carriers for Deep Chronic Wound Healing. Small, 2022, 18, e2104368.	10.0	104
6	Stabilizing Sodium Metal Anodes with Surfactant-Based Electrolytes and Unraveling the Atomic Structure of Interfaces by Cryo-TEM. Nano Letters, 2022, 22, 1382-1390.	9.1	48
7	Hydrogenation of phenol to cyclohexanol using carbon encapsulated Ni–Co alloy nanoparticles. Reaction Chemistry and Engineering, 2022, 7, 429-441.	3.7	6
8	N-doped hollow porous carbon spheres@Co Cu Fe alloy nanospheres as novel non-precious metal electrocatalysts for HER and OER. International Journal of Hydrogen Energy, 2022, 47, 5947-5960.	7.1	30
9	Synthesis of highly active carbon-encapsulated Ni ₂ P catalysts by one-step pyrolysis–phosphidation for hydrodeoxygenation of phenolic compounds. Catalysis Science and Technology, 2022, 12, 1586-1597.	4.1	8
10	Endothelialized microvessels fabricated by microfluidics facilitate osteogenic differentiation and promote bone repair. Acta Biomaterialia, 2022, 142, 85-98.	8.3	18
11	TKI resistant-based prognostic immune related gene signature in LUAD, in which FSCN1 contributes to tumor progression. Cancer Letters, 2022, 532, 215583.	7.2	17
12	Spray-On Carbon Black Nanopowder/Polyvinylidene Fluoride-Based Solar–Thermal–Electric Generators to Power Electronic Devices. ACS Applied Nano Materials, 2022, 5, 2429-2435.	5.0	4
13	Shared and disease-sensitive dysfunction across bipolar and unipolar disorder during depressive episodes: a transdiagnostic study. Neuropsychopharmacology, 2022, 47, 1922-1930.	5.4	5
14	Hemoglobin within normal range is negatively related to hemoglobin A1c in a nondiabetic American population aged 16 years and older. World Journal of Diabetes, 2022, 13, 251-259.	3.5	2
15	Targeting Endogenous Hydrogen Peroxide at Bone Defects Promotes Bone Repair (Adv. Funct. Mater.) Tj ETQq1	1	l4 rgBT /Ove
16	A Multifunctional Composite Hydrogel That Rescues the ROS Microenvironment and Guides the Immune Response for Repair of Osteoporotic Bone Defects. Advanced Functional Materials, 2022, 32, .	14.9	41
17	Ag ₃ PO ₄ Nanoparticles Decorated Carbon Nitride Nanotube to Boost Visibleâ€Light Photocatalytic Activity for the Degradation of Azo Dyes. ChemistrySelect, 2022, 7, .	1.5	6
18	Dynamic connectivity alterations in anterior cingulate cortex associated with suicide attempts in bipolar disorders with a current major depressive episode. Journal of Psychiatric Research, 2022, 149, 307-314.	3.1	7

#	Article	IF	CITATIONS
19	Ascorbic acid-induced structural defect in photocatalytic graphitic carbon nitride to boost H2O2 fuel cell performance. Journal of Power Sources, 2022, 532, 231368.	7.8	7
20	Natural proteins-derived asymmetric porous conduit for peripheral nerve regeneration. Applied Materials Today, 2022, 27, 101431.	4.3	14
21	An Investigation into the Association Between Dopamine Receptor <scp>D1</scp> Multilocus Genetic Variation, Multiparametric Magnetic Resonance Imaging, and Antidepressant Treatment. Journal of Magnetic Resonance Imaging, 2022, 56, 282-290.	3.4	1
22	Targeting Endogenous Hydrogen Peroxide at Bone Defects Promotes Bone Repair. Advanced Functional Materials, 2022, 32, .	14.9	41
23	PPy-Functionalized NiFe ₂ O ₄ Nanocomposites toward Highly Selective Pb ²⁺ Electrochemical Sensing. ACS Sustainable Chemistry and Engineering, 2022, 10, 6082-6093.	6.7	14
24	Identification of miRNA-mRNA-TF regulatory networks in peripheral blood mononuclear cells of type 1 diabetes. BMC Endocrine Disorders, 2022, 22, 119.	2.2	1
25	Reinforced Blood-Derived Protein Hydrogels Enable Dual-Level Regulation of Bio-Physiochemical Microenvironments for Personalized Bone Regeneration with Remarkable Enhanced Efficacy. Nano Letters, 2022, 22, 3904-3913.	9.1	16
26	Reaching people receiving opioid agonist therapy at community pharmacies with hepatitis C virus: an international randomised controlled trial. Alimentary Pharmacology and Therapeutics, 2022, 55, 1512-1523.	3.7	5
27	Achieving Symmetry-Breaking Charge Separation in Perylenediimide Trimers: The Effect of Bridge Resonance. Journal of Physical Chemistry B, 2022, 126, 3758-3767.	2.6	8
28	Addressable Label-Free Photoelectric Sensor Array with Self-Calibration for Detection of Neuron Specific Enolase. Analytical Chemistry, 2022, 94, 6996-7003.	6.5	13
29	Scaffolds with anisotropic structure for neural tissue engineering. Engineered Regeneration, 2022, 3, 154-162.	6.0	14
30	A MXene-derived redox homeostasis regulator perturbs the Nrf2 antioxidant program for reinforced sonodynamic therapy. Chemical Science, 2022, 13, 6704-6714.	7.4	30
31	Bi nanosphere-decorated oxygen-vacancy BiOBr hollow microspheres with exposed (110) facets to enhance the photocatalytic performance for the degradation of azo dyes. New Journal of Chemistry, 2022, 46, 12410-12418.	2.8	5
32	Regulation of differentiation of annulus fibrosus-derived stem cells using heterogeneous electrospun fibrous scaffolds. Journal of Orthopaedic Translation, 2021, 26, 171-180.	3.9	20
33	Substrate Topography Regulates Differentiation of Annulus Fibrosus-Derived Stem Cells via CAV1-YAP-Mediated Mechanotransduction. ACS Biomaterials Science and Engineering, 2021, 7, 862-871.	5.2	14
34	Efficacy and safety of sintilimab in combination with chemotherapy in previously untreated advanced or metastatic nonsquamous or squamous NSCLC: two cohorts of an open-label, phase 1b study. Cancer Immunology, Immunotherapy, 2021, 70, 857-868.	4.2	22
35	Firstâ€principles investigations on the synergistic effect of Nâ€dopant and latticeâ€strain for CO 2 reduction to CO on graphene. International Journal of Quantum Chemistry, 2021, 121, e26535.	2.0	0
36	Sonodynamic therapy reduces iron retention of hemorrhagic plaque. Bioengineering and Translational Medicine, 2021, 6, e10193.	7.1	8

#	Article	IF	CITATIONS
37	Electrochemiluminescence immunosensor based on ferrocene functionalized ZIF-8 quenching the electrochemiluminescence of Ru(bpy)32+-doped silica nanoparticles embodied N-butyl diethanolamine. Sensors and Actuators B: Chemical, 2021, 329, 129101.	7.8	14
38	Aberrant functional connectivity between the suprachiasmatic nucleus and the superior temporal gyrus: Bridging RORA gene polymorphism with diurnal mood variation in major depressive disorder. Journal of Psychiatric Research, 2021, 132, 123-130.	3.1	7
39	Characterization of the complete chloroplast genome of traditional Chinese herb, <i>Solanum japonense</i> Nakai. (Solanaceae). Mitochondrial DNA Part B: Resources, 2021, 6, 211-213.	0.4	0
40	A novel molecularly imprinted electrochemiluminescence sensor based on cobalt nitride nanoarray electrode for the sensitive detection of bisphenol S. RSC Advances, 2021, 11, 11011-11019.	3.6	7
41	Novel graphitic carbon nitride g-C ₉ N ₁₀ as a promising platform to design efficient photocatalysts for dinitrogen reduction to ammonia: the first-principles investigation. Journal of Materials Chemistry A, 2021, 9, 20615-20625.	10.3	21
42	Theoretical study on the molecular stacking interactions and charge transport properties of triazasumanene crystals – from explanation to prediction. Physical Chemistry Chemical Physics, 2021, 23, 4681-4689.	2.8	11
43	Response to Comment on "Boosted molecular mobility during common chemical reactions― Science, 2021, 371, .	12.6	20
44	Moderate mechanical stimulation rescues degenerative annulus fibrosus by suppressing caveolin-1 mediated pro-inflammatory signaling pathway. International Journal of Biological Sciences, 2021, 17, 1395-1412.	6.4	16
45	Global and reflective rumination are related to suicide attempts among patients experiencing major depressive episodes. BMC Psychiatry, 2021, 21, 117.	2.6	13
46	Predicting Neuroimaging Biomarkers for Antidepressant Selection in Early Treatment of Depression. Journal of Magnetic Resonance Imaging, 2021, 54, 551-559.	3.4	5
47	Analysis and Prediction of Significant Wave Height in the Beibu Gulf, South China Sea. Journal of Geophysical Research: Oceans, 2021, 126, e2020JC017144.	2.6	10
48	Serotonin 2A receptor polymorphism rs3803189 mediated by dynamics of default mode network: a potential biomarker for antidepressant early response. Journal of Affective Disorders, 2021, 283, 130-138.	4.1	4
49	Temporal dynamics alterations of spontaneous neuronal activity in anterior cingulate cortex predict suicidal risk in bipolar II patients. Brain Imaging and Behavior, 2021, 15, 2481-2491.	2.1	16
50	Using NMR to Test Molecular Mobility during a Chemical Reaction. Journal of Physical Chemistry Letters, 2021, 12, 2370-2375.	4.6	16
51	Metformin Carbon Dots for Promoting Periodontal Bone Regeneration via Activation of ERK/AMPK Pathway. Advanced Healthcare Materials, 2021, 10, e2100196.	7.6	32
52	MiR-34a suppression targets Nampt to ameliorate bone marrow mesenchymal stem cell senescence by regulating NAD+-Sirt1 pathway. Stem Cell Research and Therapy, 2021, 12, 271.	5.5	22
53	Proteomic Signature of Urosepsis: From Discovery in a Rabbit Model to Validation in Humans. Journal of Proteome Research, 2021, 20, 3889-3899.	3.7	4
54	Bio-inspired intestinal scavenger from microfluidic electrospray for detoxifying lipopolysaccharide. Bioactive Materials, 2021, 6, 1653-1662.	15.6	35

#	Article	IF	CITATIONS
55	Recognize the role of CD146/MCAM in the osteosarcoma progression: an in vitro study. Cancer Cell International, 2021, 21, 300.	4.1	4
56	Reply to Comment on "Using NMR to Test Molecular Mobility during a Chemical Reaction― Journal of Physical Chemistry Letters, 2021, 12, 5744-5747.	4.6	9
57	PTEN suppresses tumorigenesis by directly dephosphorylating Akt. Signal Transduction and Targeted Therapy, 2021, 6, 262.	17.1	8
58	Sexâ€specific differences in blood lipids and lipid ratios in typeÂ2 diabetic foot patients. Journal of Diabetes Investigation, 2021, , .	2.4	3
59	Subâ€second transient activated patterns to sad expressions in major depressive disorders discovered via hidden Markov model. Journal of Neuroscience Research, 2021, 99, 3250-3260.	2.9	6
60	PDI hexamer based on combination of direct and indirect linkage manners for nonâ€fullerene organic solar cells. Chemistry - an Asian Journal, 2021, 16, 3767-3773.	3.3	3
61	Molecules, the Ultimate Nanomotor: Linking Chemical Reaction Intermediates to their Molecular Diffusivity. ACS Nano, 2021, 15, 14947-14953.	14.6	15
62	Enzyme-functionalized structural color hydrogel particles for urea detection and elimination. Journal of Cleaner Production, 2021, 315, 128149.	9.3	28
63	Multiplex assays of bladder cancer protein markers with magnetic structural color hydrogel microcarriers based on microfluidics. Sensors and Actuators B: Chemical, 2021, 346, 130464.	7.8	22
64	Quantitative analysis of the profiles of twelve major compounds in Gentiana straminea Maxim. Roots by LC-MS/MS in an extensive germplasm survey in the Qinghai-Tibetan plateau. Journal of Ethnopharmacology, 2021, 280, 114068.	4.1	12
65	Highly sensitive and selective electrochemical sensor based on porous graphitic carbon nitride/CoMn2O4 nanocomposite toward heavy metal ions. Sensors and Actuators B: Chemical, 2021, 346, 130539.	7.8	46
66	Total syntheses of melodienones by redox isomerization of propargylic alcohols. Organic and Biomolecular Chemistry, 2021, 19, 5077-5081.	2.8	2
67	Highly efficient hydrogenation of phenol to cyclohexanol over Ni-based catalysts derived from Ni-MOF-74. Reaction Chemistry and Engineering, 2021, 7, 170-180.	3.7	14
68	The Genetic Diversity of the Rice-crayfish Eco-farming Procambarus clarkii in Anhui Province, China. Turkish Journal of Fisheries and Aquatic Sciences, 2021, 22, .	0.9	3
69	Carbonic anhydrase 12 gene silencing reverses the sensitivity of paclitaxel in drug-resistant breast cancer cells. Bioengineered, 2021, 12, 9806-9818.	3.2	6
70	Unraveling an Innate Mechanism of Pathological Mineralizationâ€Regulated Inflammation by a Nanobiomimetic System. Advanced Healthcare Materials, 2021, 10, e2101586.	7.6	6
71	A double dose of advice. Science, 2021, , .	12.6	0
72	Assessment of TMB, PD-L1, and lymphocyte to monocyte ratio as predictive potential in a phase Ib study of sintilimab in patients with advanced solid tumors. American Journal of Cancer Research, 2021, 11, 4259-4276.	1.4	1

#	Article	IF	CITATIONS
73	Responsive Janus Structural Color Hydrogel Micromotors for Label-Free Multiplex Assays. Research, 2021, 2021, 9829068.	5.7	24
74	A pre-operative prognostic model predicting all cause and cause specific mortality for women presenting with invasive breast cancer. Breast, 2021, 61, 11-21.	2.2	0
75	SET activation of nitroarenes by 2-azaallyl anions as a straightforward access to 2,5-dihydro-1,2,4-oxadiazoles. Nature Communications, 2021, 12, 7060.	12.8	7
76	Microfluidic electrospray photo-crosslinkable κ-Carrageenan microparticles for wound healing. Engineered Regeneration, 2021, 2, 257-262.	6.0	48
77	Facile fabrication of superhydrophobic Titanium dioxide-composited cotton fabrics to realize oil-water separation with efficiently photocatalytic degradation for water-soluble pollutants. Colloids and Surfaces A: Physicochemical and Engineering Aspects, 2020, 585, 124080.	4.7	44
78	WNT1â€inducible signaling proteinâ€1 mediates TGFâ€î21â€induced renal fibrosis in tubular epithelial cells and unilateral ureteral obstruction mouse models via autophagy. Journal of Cellular Physiology, 2020, 235, 2009-2022.	4.1	34
79	Immunotherapeutic silk inverse opal particles for post-surgical tumor treatment. Science Bulletin, 2020, 65, 380-388.	9.0	73
80	Anisotropic structural color particles from colloidal phase separation. Science Advances, 2020, 6, eaay1438.	10.3	133
81	Enabling high-performance sodium metal anodes via A sodiophilic structure constructed by hierarchical Sb2MoO6 microspheres. Nano Energy, 2020, 69, 104446.	16.0	43
82	A photoelectrochemical immunosensor based on CdS/CdTe-cosensitized SnO ₂ as a platform for the ultrasensitive detection of amyloid \hat{I}^2 -protein. Analyst, The, 2020, 145, 619-625.	3.5	19
83	Characterization of the complete chloroplast genome of traditional Tibetan herb,Rheum PumilumMaxim. (Polygonaceae). Mitochondrial DNA Part B: Resources, 2020, 5, 133-135.	0.4	1
84	Stomatocyte structural color-barcode micromotors for multiplex assays. National Science Review, 2020, 7, 644-651.	9.5	56
85	Myeloid FBW7 deficiency disrupts redox homeostasis and aggravates dietary-induced insulin resistance. Redox Biology, 2020, 37, 101688.	9.0	18
86	Graphitic Carbon Nitride-Based Photocatalytic Materials: Preparation Strategy and Application. ACS Sustainable Chemistry and Engineering, 2020, 8, 16048-16085.	6.7	96
87	Signal-off electrochemiluminescence immunosensor based on Mn-Eumelanin coordination nanoparticles quenching PtCo-CuFe2O4-reduced graphene oxide enhanced luminol. Sensors and Actuators B: Chemical, 2020, 323, 128702.	7.8	10
88	Aberrant functional connectivity and graph properties in bipolar II disorder with suicide attempts. Journal of Affective Disorders, 2020, 275, 202-209.	4.1	16
89	Electrochemical chiral amino acid biosensor based on dopamine-localized gold nanoparticles @ left-handed spiral chiral carbon nanotubes. Analytical Methods, 2020, 12, 3901-3908.	2.7	6
90	Boosted molecular mobility during common chemical reactions. Science, 2020, 369, 537-541.	12.6	62

#	Article	IF	CITATIONS
91	Phenol-like group functionalized graphene quantum dots structurally mimicking natural antioxidants for highly efficient acute kidney injury treatment. Chemical Science, 2020, 11, 12721-12730.	7.4	54
92	Safety and efficacy of sintilimab combined with oxaliplatin/capecitabine as first-line treatment in patients with locally advanced or metastatic gastric/gastroesophageal junction adenocarcinoma in a phase Ib clinical trial. BMC Cancer, 2020, 20, 760.	2.6	43
93	Photo-switchable electron-transporting layers for self-driven perovskite photodetectors towards high detectivity. Journal of Materials Chemistry C, 2020, 8, 16506-16512.	5.5	10
94	A novel approach to photoelectrochemical immunoassay for procalcitonin on the basis of SnS ₂ /CdS. New Journal of Chemistry, 2020, 44, 15281-15288.	2.8	5
95	Distance-based quantification of miRNA-21 by the coffee-ring effect using paper devices. Mikrochimica Acta, 2020, 187, 513.	5.0	18
96	Tunable MXene-Derived 1D/2D Hybrid Nanoarchitectures as a Stable Matrix for Dendrite-Free and Ultrahigh Capacity Sodium Metal Anode. Nano Letters, 2020, 20, 7700-7708.	9.1	110
97	The Ubiquitin E3 Ligase Parkin Inhibits Innate Antiviral Immunity Through K48-Linked Polyubiquitination of RIG-I and MDA5. Frontiers in Immunology, 2020, 11, 1926.	4.8	17
98	Discriminating Suicide Attempters and Predicting Suicide Risk Using Altered Frontolimbic Resting-State Functional Connectivity in Patients With Bipolar II Disorder. Frontiers in Psychiatry, 2020, 11, 597770.	2.6	12
99	Gradually evaluating of suicidal risk in depression by semi-supervised cluster analysis on resting-state fMRI. Brain Imaging and Behavior, 2020, 15, 2149-2158.	2.1	9
100	Shape memory graphene and cutting-edge achievements. APL Materials, 2020, 8, .	5.1	12
101	Interfacial structure design of <scp>MXeneâ€based</scp> nanomaterials for electrochemical energy storage and conversion. InformaÄnÃ-Materiály, 2020, 2, 1057-1076.	17.3	143
102	Antigen down format photoelectrochemical analysis supported by fullerene functionalized Sn ₃ O ₄ . Chemical Communications, 2020, 56, 7455-7458.	4.1	19
103	Combining theories and experiments to understand the sodium nucleation behavior towards safe sodium metal batteries. Chemical Society Reviews, 2020, 49, 3783-3805.	38.1	161
104	Oriented boronate affinity–imprinted inverse opal hydrogel for glycoprotein assay via colorimetry. Mikrochimica Acta, 2020, 187, 348.	5.0	36
105	Biomimetic periosteum-bone substitute composed of preosteoblast-derived matrix and hydrogel for large segmental bone defect repair. Acta Biomaterialia, 2020, 113, 317-327.	8.3	55
106	Biomimetic bone regeneration using angle-ply collagen membrane-supported cell sheets subjected to mechanical conditioning. Acta Biomaterialia, 2020, 112, 75-86.	8.3	23
107	Facile-Processed Nanocarbon-Promoted Sulfur Cathode for Highly Stable Sodium-Sulfur Batteries. Cell Reports Physical Science, 2020, 1, 100015.	5.6	18
108	Ni–Fe nanocubes embedded with Pt nanoparticles for hydrogen and oxygen evolution reactions. International Journal of Hydrogen Energy, 2020, 45, 20832-20842.	7.1	40

#	Article	IF	CITATIONS
109	Transition Metalâ€Free Aroylation of Diarylmethanes with <i>N</i> â€Bnâ€ <i>N</i> â€Boc Arylamides and <i>N</i> â€Acylpyrroles. Advanced Synthesis and Catalysis, 2020, 362, 3423-3430.	4.3	20
110	Structural–functional decoupling predicts suicide attempts in bipolar disorder patients with a current major depressive episode. Neuropsychopharmacology, 2020, 45, 1735-1742.	5.4	25
111	Attenuated Salmonella engineered with an apoptosis-inducing factor (AIF) eukaryotic expressing system enhances its anti-tumor effect in melanoma in vitro and in vivo. Applied Microbiology and Biotechnology, 2020, 104, 3517-3528.	3.6	11
112	Complete chloroplast genome of <i>Meconopsis integrifolia</i> (Papaveraceae). Mitochondrial DNA Part B: Resources, 2020, 5, 142-144.	0.4	1
113	Three-Dimensional Porous Nitrogen-Doped Carbon Nanosheet with Embedded Ni _{<i>x</i>} Co _{3–<i>x</i>} S ₄ Nanocrystals for Advanced Lithium–Sulfur Batteries. ACS Applied Materials & Interfaces, 2020, 12, 9181-9189.	8.0	36
114	Signal-off electrochemiluminescence immunosensors based on the quenching effect between curcumin-conjugated Au nanoparticles encapsulated in ZIF-8 and CdS-decorated TiO ₂ nanobelts for insulin detection. Analyst, The, 2020, 145, 1858-1864.	3.5	11
115	Multistep Reaction Pathway for CO 2 Reduction on Hydrideâ€Capped Si Nanosheets. ChemCatChem, 2020, 12, 722-725.	3.7	1
116	Label-free electrochemical immunosensor based on biocompatible nanoporous Fe ₃ O ₄ and biotin–streptavidin system for sensitive detection of zearalenone. Analyst, The, 2020, 145, 1368-1375.	3.5	50
117	Effects of Matrix Stiffness on the Differentiation of Multipotent Stem Cells. Current Stem Cell Research and Therapy, 2020, 15, 449-461.	1.3	14
118	Comparison of Profiling of Hairy Root of Two Tibetan Medicinal Plants Przewalskia tangutica Maxim. and Anisodus tanguticus Maxim. Current Pharmaceutical Biotechnology, 2020, 21, 516-527.	1.6	2
119	Identification of Small-Molecule Regulators of Testicular Receptor 4 via a Drug Repurposing Screening. ACS Omega, 2020, 5, 30625-30632.	3.5	Ο
120	Identification of Small-Molecule Regulators of Testicular Receptor 4 via a Drug Repurposing Screening. ACS Omega, 2020, 5, 30625-30632.	3.5	3
121	Rapid inhibition of atherosclerotic plaque progression by sonodynamic therapy. Cardiovascular Research, 2019, 115, 190-203.	3.8	49
122	Renal-Clearable Porphyrinic Metal–Organic Framework Nanodots for Enhanced Photodynamic Therapy. ACS Nano, 2019, 13, 9206-9217.	14.6	110
123	Early identification of bipolar from unipolar depression before manic episode: Evidence from dynamic rfMRI. Bipolar Disorders, 2019, 21, 774-784.	1.9	32
124	Fe2O3 and Co bimetallic decorated nitrogen doped graphene nanomaterial for effective electrochemical water split hydrogen evolution reaction. Journal of Electroanalytical Chemistry, 2019, 849, 113345.	3.8	14
125	An ultrasensitive label-free photoelectrochemical sensor based on Ag ₂ O-sensitized WO ₃ /TiO ₂ acicular composite for AFB1 detection. Analytical Methods, 2019, 11, 3890-3897.	2.7	22
126	Ring fusion attenuates the device performance: star-shaped long helical perylene diimide based non-fullerene acceptors. Journal of Materials Chemistry C, 2019, 7, 9564-9572.	5.5	25

#	Article	IF	CITATIONS
127	Superâ€Elastic Magnetic Structural Color Hydrogels. Small, 2019, 15, e1902198.	10.0	89
128	Accurate Binding Energies for Lithium Polysulfides and Assessment of Density Functionals for Lithium–Sulfur Battery Research. Journal of Physical Chemistry C, 2019, 123, 20737-20747.	3.1	34
129	Remote and reversible control of in vivo bacteria clustering by NIR-driven multivalent upconverting nanosystems. Biomaterials, 2019, 217, 119310.	11.4	20
130	Plasmonic Pt Superstructures with Boosted Nearâ€Infrared Absorption and Photothermal Conversion Efficiency in the Second Biowindow for Cancer Therapy. Advanced Materials, 2019, 31, e1904836.	21.0	105
131	Direct Nanoscopic Measurement of Laminar Slip Flow Penetration of Deformable Polymer Brush Surfaces: Synergistic Effect of Grafting Density and Solvent Quality. Langmuir, 2019, 35, 13646-13655.	3.5	7
132	Defectâ€Rich Adhesive Nanozymes as Efficient Antibiotics for Enhanced Bacterial Inhibition. Angewandte Chemie, 2019, 131, 16382-16388.	2.0	11
133	Room temperature synthesis of Cu[Fe(CN)6]·XH2O cube derived ferric oxide@cupric oxide alloy ball on nitrogen-doped graphene as highly efficient electrochemical water splitting. International Journal of Hydrogen Energy, 2019, 44, 28543-28555.	7.1	2
134	Defectâ€Rich Adhesive Nanozymes as Efficient Antibiotics for Enhanced Bacterial Inhibition. Angewandte Chemie - International Edition, 2019, 58, 16236-16242.	13.8	246
135	Integrated Effects of Near-Field Enhancement-Induced Excitation and Surface Plasmon-Coupled Emission of Elongated Gold Nanocrystals on Fluorescence Enhancement and the Applications in PLEDs. ACS Applied Electronic Materials, 2019, 1, 2116-2123.	4.3	21
136	Emerging barcode particles for multiplex bioassays. Science China Materials, 2019, 62, 289-324.	6.3	43
137	Charge transport properties in organic D-A mixed-stack complexes based on corannulene and sumanene derivatives-a theoretical study. Organic Electronics, 2019, 68, 35-44.	2.6	19
138	Historical population decline and habitat loss in a critically endangered species, the Chinese alligator (Alligator sinensis). Global Ecology and Conservation, 2019, 20, e00692.	2.1	7
139	Novel potential and current type chiral amino acids biosensor based on L/D-handed double helix carbon nanotubes@polypyrrole@Au nanoparticles@L/D-cysteine. Sensors and Actuators B: Chemical, 2019, 296, 126667.	7.8	21
140	Enabling Safe Sodium Metal Batteries by Solid Electrolyte Interphase Engineering: A Review. Industrial & Engineering Chemistry Research, 2019, 58, 9758-9780.	3.7	88
141	Increased hepcidin in hemorrhagic plaques correlates with iron-stimulated IL-6/STAT3 pathway activation in macrophages. Biochemical and Biophysical Research Communications, 2019, 515, 394-400.	2.1	11
142	Porphyrin MOF Dots–Based, Functionâ€Adaptive Nanoplatform for Enhanced Penetration and Photodynamic Eradication of Bacterial Biofilms. Advanced Functional Materials, 2019, 29, 1903018.	14.9	175
143	Exercise Attenuates Acute β-Adrenergic Overactivation–Induced Cardiac Fibrosis by Modulating Cytokines. Journal of Cardiovascular Translational Research, 2019, 12, 528-538.	2.4	19
144	Adaptation of Human iPSC-Derived Cardiomyocytes to Tyrosine Kinase Inhibitors Reduces Acute Cardiotoxicity via Metabolic Reprogramming. Cell Systems, 2019, 8, 412-426.e7.	6.2	49

#	Article	IF	CITATIONS
145	Graphene hybrid colloidal crystal arrays with photo-controllable structural colors. Nanoscale, 2019, 11, 10846-10851.	5.6	35
146	Polydopamine-assisted surface modification for orthopaedic implants. Journal of Orthopaedic Translation, 2019, 17, 82-95.	3.9	91
147	Condensing-enriched magnetic photonic barcodes on superhydrophobic surface for ultrasensitive multiple detection. Lab on A Chip, 2019, 19, 1783-1789.	6.0	15
148	Rapid and Scalable Synthesis of Cuprous Halide-Derived Copper Nano-Architectures for Selective Electrochemical Reduction of Carbon Dioxide. Nano Letters, 2019, 19, 3925-3932.	9.1	78
149	Pâ€Glycoprotein Antibody Decorated Porous Hydrogel Particles for Capture and Release of Drugâ€Resistant Tumor Cells. Advanced Healthcare Materials, 2019, 8, e1900136.	7.6	22
150	Conductive Polymer Hydrogel Microfibers from Multiflow Microfluidics. Small, 2019, 15, e1805162.	10.0	59
151	Adaptive Zeroing-Gradient Controller for Ship Course Tracking With Near Singularity Considered and Zero Theoretical Tracking Error. IEEE Access, 2019, 7, 38205-38212.	4.2	7
152	Construction of Nanozymeâ€Hydrogel for Enhanced Capture and Elimination of Bacteria. Advanced Functional Materials, 2019, 29, 1900518.	14.9	213
153	Nip the Sodium Dendrites in the Bud on Planar Doped Graphene in Liquid/Gel Electrolytes. Advanced Functional Materials, 2019, 29, 1807974.	14.9	45
154	Template-Free Controllable Electrochemical Synthesis of Hierarchical Flower-Like Platinum Nanoparticles/Nitrogen Doped Helical Carbon Nanotubes for Label-Free Biosensing of Bovine Serum Albumin. Journal of the Electrochemical Society, 2019, 166, B117-B124.	2.9	11
155	Ultrasensitive magnetic resonance imaging of systemic reactive oxygen species <i>in vivo</i> for early diagnosis of sepsis using activatable nanoprobes. Chemical Science, 2019, 10, 3770-3778.	7.4	37
156	Porous Polyvinylidene Fluoride Thin-Film Sensors from Colloidal Crystal Templates. Journal of Nanoscience and Nanotechnology, 2019, 19, 8104-8111.	0.9	5
157	A high-mobility, high-luminescence and low-threshold pentacene-doped cyano-substituted distyrylbenzene crystal. Journal of Materials Chemistry C, 2019, 7, 13447-13453.	5.5	9
158	Delta-Aminolevulinic Acid-Mediated Photodiagnoses in Surgical Oncology: A Historical Review of Clinical Trials. Frontiers in Surgery, 2019, 6, 45.	1.4	16
159	Cardiomyocytesâ€Actuated <i>Morpho</i> Butterfly Wings. Advanced Materials, 2019, 31, e1805431.	21.0	129
160	Pillared MXene with Ultralarge Interlayer Spacing as a Stable Matrix for High Performance Sodium Metal Anodes. Advanced Functional Materials, 2019, 29, 1805946.	14.9	242
161	Graphene Regulated Ceramic Electrolyte for Solid-State Sodium Metal Battery with Superior Electrochemical Stability. ACS Applied Materials & amp; Interfaces, 2019, 11, 5064-5072.	8.0	77
	Comparison of intestinal microbes in female and male Chinese concaveâ€eared frogs (<i>Odorrana) Tj ETQq0 0</i>	0 rgBT /O	verlock 10 Tf

162

#	Article	IF	CITATIONS
163	Frogspawnâ€Coralâ€Like Hollow Sodium Sulfide Nanostructured Cathode for Highâ€Rate Performance Sodium–Sulfur Batteries. Advanced Energy Materials, 2019, 9, 1803251.	19.5	59
164	Association of serum lipids with clinical outcome in acute ischaemic stroke: A systematic review and meta-analysis. Journal of Clinical Neuroscience, 2019, 59, 236-244.	1.5	16
165	Carbon quantum dots encapsulated in super small platinum nanocrystals core-shell architecture/nitrogen doped graphene hybrid nanocomposite for electrochemical biosensing of DNA damage biomarker-8-hydroxy-2′-deoxyguanosine. Analytica Chimica Acta, 2019, 1047, 9-20.	5.4	20
166	Specific Oxygenated Groups Enriched Graphene Quantum Dots as Highly Efficient Enzyme Mimics. Small, 2018, 14, e1703710.	10.0	92
167	Porous Hydrogel Encapsulated Photonic Barcodes for Multiplex MicroRNA Quantification. Advanced Functional Materials, 2018, 28, 1704458.	14.9	56
168	β-arrestin2 functions as a key regulator in the sympathetic-triggered immunodepression after stroke. Journal of Neuroinflammation, 2018, 15, 102.	7.2	19
169	Egg Component-Composited Inverse Opal Particles for Synergistic Drug Delivery. ACS Applied Materials & Interfaces, 2018, 10, 17058-17064.	8.0	22
170	Genetic transformation of the endangered Tibetan medicinal plant Przewalskia tangutica Maxim and alkaloid production profiling revealed by HPLC. 3 Biotech, 2018, 8, 179.	2.2	3
171	Recent progress in organometal halide perovskite photodetectors. Organic Electronics, 2018, 52, 172-183.	2.6	83
172	Aptamer-based hydrogel barcodes for the capture and detection of multiple types of pathogenic bacteria. Biosensors and Bioelectronics, 2018, 100, 404-410.	10.1	86
173	Down's syndrome screening with hydrogel photonic barcodes. Sensors and Actuators B: Chemical, 2018, 255, 2690-2696.	7.8	12
174	Bioinspired Photonic Barcodes: Bioinspired Photonic Barcodes with Graphene Oxide Encapsulation for Multiplexed MicroRNA Quantification (Small 52/2018). Small, 2018, 14, 1870255.	10.0	2
175	A novel label-free photoelectrochemical immunosensor based on NCQDs and Bi ₂ S ₃ co-sensitized hierarchical mesoporous SnO ₂ microflowers for detection of NT-proBNP. Journal of Materials Chemistry B, 2018, 6, 7634-7642.	5.8	26
176	Bioinspired Photonic Barcodes with Graphene Oxide Encapsulation for Multiplexed MicroRNA Quantification. Small, 2018, 14, e1803551.	10.0	46
177	Multifunctional Chitosan Inverse Opal Particles for Wound Healing. ACS Nano, 2018, 12, 10493-10500.	14.6	141
178	Chiral Ramachandran Plots II: General Trends and Protein Chirality Spectra. Biochemistry, 2018, 57, 6395-6403.	2.5	8
179	Sonodynamic therapy-induced foam cells apoptosis activates the phagocytic PPARÎ ³ -LXRα-ABCA1/ABCG1 pathway and promotes cholesterol efflux in advanced plaque. Theranostics, 2018, 8, 4969-4984.	10.0	66
180	Composite Multifunctional Micromotors from Droplet Microfluidics. ACS Applied Materials & Interfaces, 2018, 10, 34618-34624.	8.0	42

#	Article	IF	CITATIONS
181	Mesoporous Colloidal Photonic Crystal Particles for Intelligent Drug Delivery. ACS Applied Materials & Interfaces, 2018, 10, 33936-33944.	8.0	38
182	A Chemically Engineered Porous Copper Matrix with Cylindrical Core–Shell Skeleton as a Stable Host for Metallic Sodium Anodes. Advanced Functional Materials, 2018, 28, 1802282.	14.9	104
183	Unraveling the Enzymatic Activity of Oxygenated Carbon Nanotubes and Their Application in the Treatment of Bacterial Infections. Nano Letters, 2018, 18, 3344-3351.	9.1	199
184	Convenient one step synthesis of molybdenum carbide embedded N-doped carbon nanolayer hybrid architecture using cheap cotton as precursor for efficient hydrogen evolution. Journal of Electroanalytical Chemistry, 2018, 824, 207-215.	3.8	4
185	Multicolored photonic barcodes from dynamic micromolding. Materials Horizons, 2018, 5, 979-983.	12.2	40
186	The Short-term Prognostic Value of the Triglyceride-to-high-density Lipoprotein Cholesterol Ratio in Acute Ischemic Stroke. , 2018, 9, 498.		31
187	Nitrogen doped chiral carbonaceous nanotube for ultrasensitive DNA direct electrochemistry, DNA hybridization and damage study. Analytica Chimica Acta, 2018, 1038, 41-51.	5.4	3
188	Differential long noncoding RNA expressions in peripheral blood mononuclear cells for detection of acute ischemic stroke. Clinical Science, 2018, 132, 1597-1614.	4.3	46
189	Quantum-dot-encapsulated core–shell barcode particles from droplet microfluidics. Journal of Materials Chemistry B, 2018, 6, 7257-7262.	5.8	28
190	Integrated analysis of mRNA and miRNA expression profiles reveals muscle growth differences between adult female and male Chinese concave-eared frogs (Odorrana tormota). Gene, 2018, 678, 241-251.	2.2	14
191	Template, surfactant, stabilizer free controllable synthesis of various morphologies platinum decorated ordered mesoporous carbon nano architecture for high–performance electrochemical sensing. Journal of Electroanalytical Chemistry, 2018, 825, 40-50.	3.8	2
192	Two introduced crocodile species had changed reproductive characteristics in China. Animal Reproduction Science, 2018, 196, 150-159.	1.5	2
193	Biomimetic enzyme cascade reaction system in microfluidic electrospray microcapsules. Science Advances, 2018, 4, eaat2816.	10.3	277
194	Folic Acid-Functionalized Hybrid Photonic Barcodes for Capture and Release of Circulating Tumor Cells. ACS Applied Materials & amp; Interfaces, 2018, 10, 21206-21212.	8.0	46
195	Design synthesis of a controllable flower-like Pt-graphene oxide architecture through electrostatic self-assembly for DNA damage biomarker 8-hydroxy-2′-deoxyguanosine biosensing research. Analyst, The, 2018, 143, 3619-3627.	3.5	8
196	Cuttlefish Ink Tagged Photonic Crystal Particles and Their Ion-Responsive Construction. Journal of Nanoscience and Nanotechnology, 2018, 18, 4834-4840.	0.9	5
197	Substrate Doping Effect and Unusually Large Angle van Hove Singularity Evolution in Twisted Bi―and Multilayer Graphene. Advanced Materials, 2017, 29, 1606741.	21.0	43
198	Formation mechanism of overlapping grain boundaries in graphene chemical vapor deposition growth. Chemical Science, 2017, 8, 2209-2214.	7.4	35

#	Article	IF	CITATIONS
199	Bio-inspired self-healing structural color hydrogel. Proceedings of the National Academy of Sciences of the United States of America, 2017, 114, 5900-5905.	7.1	248
200	Hyaluronic Acid-Templated Ag Nanoparticles/Graphene Oxide Composites for Synergistic Therapy of Bacteria Infection. ACS Applied Materials & Interfaces, 2017, 9, 19717-19724.	8.0	110
201	Rapid growth of angle-confined large-domain graphene bicrystals. Nano Research, 2017, 10, 1189-1199.	10.4	9
202	Enzymatic Inverse Opal Hydrogel Particles for Biocatalyst. ACS Applied Materials & Interfaces, 2017, 9, 12914-12918.	8.0	65
203	Reinvestigation of the Infrared Spectrum of the Gas-Phase Protonated Water Tetramer. Journal of Physical Chemistry A, 2017, 121, 3056-3070.	2.5	24
204	Multiple paternity: A compensation mechanism of the Chinese alligator for inbreeding. Animal Reproduction Science, 2017, 187, 124-132.	1.5	8
205	Antibacterial Structural Color Hydrogels. ACS Applied Materials & Interfaces, 2017, 9, 38901-38907.	8.0	34
206	Bioinspired Heterogeneous Structural Color Stripes from Capillaries. Advanced Materials, 2017, 29, 1704569.	21.0	123
207	Critical Role of Ultrathin Graphene Films with Tunable Thickness in Enabling Highly Stable Sodium Metal Anodes. Nano Letters, 2017, 17, 6808-6815.	9.1	204
208	Responsive photonic barcodes for sensitive multiplex bioassay. Nanoscale, 2017, 9, 14111-14117.	5.6	21
209	Chiral Ramachandran Plots I: Glycine. Biochemistry, 2017, 56, 5635-5643.	2.5	10
210	Molecular characterization and tissue expression profiles of prepro-vasoactive intestinal peptide in the Chinese alligator (<i>Alligator sinensis</i>) during the active and hibernating periods. Journal of Experimental Zoology Part A: Ecological and Integrative Physiology, 2017, 327, 79-88.	1.9	2
211	Microfluidic Lithography of Bioinspired Helical Micromotors. Angewandte Chemie - International Edition, 2017, 56, 12127-12131.	13.8	126
212	Microfluidic Lithography of Bioinspired Helical Micromotors. Angewandte Chemie, 2017, 129, 12295-12299.	2.0	37
213	Perovskite-based photodetectors: materials and devices. Chemical Society Reviews, 2017, 46, 5204-5236.	38.1	709
214	Accuracy of M2BPGi, compared with Fibro Scan®, in analysis of liver fibrosis in patients with hepatitis C. BMC Gastroenterology, 2017, 17, 62.	2.0	37
215	Hybrid hydrogel photonic barcodes for multiplex detection of tumor markers. Biosensors and Bioelectronics, 2017, 87, 264-270.	10.1	60
216	Immunohistochemical Localization of Somatostatin in the Brain of Chinese Alligator <i>Alligator sinensis</i> . Anatomical Record, 2017, 300, 507-519.	1.4	2

#	Article	IF	CITATIONS
217	Tuning Chemical Potential Difference across Alternately Doped Graphene p–n Junctions for High-Efficiency Photodetection. Nano Letters, 2016, 16, 4094-4101.	9.1	34
218	Cells Cultured on Core–Shell Photonic Crystal Barcodes for Drug Screening. ACS Applied Materials & Interfaces, 2016, 8, 13840-13848.	8.0	102
219	Red Blood Cell Distribution Width to Platelet Ratio is Related to Histologic Severity of Primary Biliary Cirrhosis. Medicine (United States), 2016, 95, e3114.	1.0	38
220	Complete Assignment of the Infrared Spectrum of the Gas-Phase Protonated Ammonia Dimer. Journal of Physical Chemistry A, 2016, 120, 3117-3135.	2.5	19
221	Building Large-Domain Twisted Bilayer Graphene with van Hove Singularity. ACS Nano, 2016, 10, 6725-6730.	14.6	53
222	Metabolically Obese Individuals of Normal Weight Have a High Risk of 25-Hydroxyvitamin D Deficiency. American Journal of the Medical Sciences, 2016, 352, 360-367.	1.1	8
223	Raman spectroscopic characterization of stacking configuration and interlayer coupling of twisted multilayer graphene grown by chemical vapor deposition. Carbon, 2016, 110, 225-231.	10.3	28
224	Ultrafast growth of single-crystal graphene assisted by a continuous oxygen supply. Nature Nanotechnology, 2016, 11, 930-935.	31.5	330
225	Surface Monocrystallization of Copper Foil for Fast Growth of Large Singleâ€Crystal Graphene under Free Molecular Flow. Advanced Materials, 2016, 28, 8968-8974.	21.0	128
226	Selectively enhanced photocurrent generation in twisted bilayer graphene with van Hove singularity. Nature Communications, 2016, 7, 10699.	12.8	136
227	Tubular inverse opal scaffolds for biomimetic vessels. Nanoscale, 2016, 8, 13574-13580.	5.6	28
228	Blocking Sympathetic Nervous System Reverses Partially Stroke-Induced Immunosuppression but does not Aggravate Functional Outcome After Experimental Stroke in Rats. Neurochemical Research, 2016, 41, 1877-1886.	3.3	18
229	Boronate affinity molecularly imprinted inverse opal particles for multiple label-free bioassays. Chemical Communications, 2016, 52, 3296-3299.	4.1	53
230	A photonic crystal hydrogel suspension array for the capture of blood cells from whole blood. Nanoscale, 2016, 8, 3841-3847.	5.6	44
231	A novel Mn 2+ -doped core/shell quantum dot-based intracellular probe for fluoride anions sensing in MC3T3-E1 osteoblastic cells. Talanta, 2016, 149, 285-289.	5.5	6
232	Free-Standing Photonic Crystal Films with Gradient Structural Colors. ACS Applied Materials & Interfaces, 2016, 8, 6796-6801.	8.0	62
233	A highly luminescent organic crystal with the well-balanced charge transport property: The role of cyano-substitution in the terminal phenyl unit of distyrylbenzene. Organic Electronics, 2016, 28, 287-293.	2.6	8
234	Mechanisms of Intracellular Calcium Homeostasis in MC3T3-E1 Cells and Bone Tissues of Sprague-Dawley Rats Exposed to Fluoride. Biological Trace Element Research, 2016, 170, 331-339.	3.5	8

#	Article	IF	CITATIONS
235	Potential specific immunological indicators for stroke associated infection are partly modulated by sympathetic pathway activation. Oncotarget, 2016, 7, 52404-52415.	1.8	11
236	Colorimetric logic response based on aptamer functionalized colloidal crystal hydrogels. Nanoscale, 2015, 7, 7565-7568.	5.6	25
237	Multifunctional inverse opal particles for drug delivery and monitoring. Nanoscale, 2015, 7, 10590-10594.	5.6	93
238	Photonic Crystal Microbubbles as Suspension Barcodes. Journal of the American Chemical Society, 2015, 137, 15533-15539.	13.7	117
239	Protonated Water Dimer on Benzene: Standing Eigen or Crouching Zundel?. Journal of Physical Chemistry B, 2015, 119, 2658-2667.	2.6	15
240	Controlled synthesis of single-crystal SnSe nanoplates. Nano Research, 2015, 8, 288-295.	10.4	207
241	The multifaceted role of CD146/MCAM in the promotion of melanoma progression. Cancer Cell International, 2015, 15, 3.	4.1	49
242	van Hove Singularity Enhanced Photochemical Reactivity of Twisted Bilayer Graphene. Nano Letters, 2015, 15, 5585-5589.	9.1	59
243	Discovery of Imidazo[1,2-α][1,8]naphthyridine Derivatives as Potential HCV Entry Inhibitor. ACS Medicinal Chemistry Letters, 2015, 6, 977-981.	2.8	19
244	Cardiac valve cells and their microenvironment—insights from in vitro studies. Nature Reviews Cardiology, 2014, 11, 715-727.	13.7	80
245	Identification and localization of gastrointestinal hormones in the skin of the bullfrog Rana catesbeiana during periods of activity and hibernation. Acta Histochemica, 2014, 116, 1418-1426.	1.8	4
246	The Predominant Pathway of Apoptosis in THP-1 Macrophage-Derived Foam Cells Induced by 5-Aminolevulinic Acid-Mediated Sonodynamic Therapy is the Mitochondria-Caspase Pathway Despite the Participation of Endoplasmic Reticulum Stress. Cellular Physiology and Biochemistry, 2014, 33, 1789-1801.	1.6	55
247	Quantum-dot-tagged photonic crystal beads for multiplex detection of tumor markers. Chemical Communications, 2014, 50, 14589-14592.	4.1	33
248	Fluorescence energy transfer-based multiplexed hybridization assay using gold nanoparticles and quantum dot conjugates on photonic crystal beads. Mikrochimica Acta, 2014, 181, 1109-1115.	5.0	12
249	Roles of transforming growth factorâ€Î²1 and OBâ€cadherin in porcine cardiac valve myofibroblast differentiation. FASEB Journal, 2014, 28, 4551-4562.	0.5	32
250	Distribution of endocrine cells in the digestive tract of Alligator sinensis during the active and hibernating period. Tissue and Cell, 2014, 46, 343-351.	2.2	5
251	Plasmon-Enhanced Photothermoelectric Conversion in Chemical Vapor Deposited Graphene p–n Junctions. Journal of the American Chemical Society, 2013, 135, 10926-10929.	13.7	61
252	Photoinduced Methylation of Graphene. Small, 2013, 9, 1348-1352.	10.0	29

#	Article	IF	CITATIONS
253	Synthesis of Boronâ€Doped Graphene Monolayers Using the Sole Solid Feedstock by Chemical Vapor Deposition. Small, 2013, 9, 1316-1320.	10.0	181
254	Hydrogels preserve native phenotypes of valvular fibroblasts through an elasticity-regulated PI3K/AKT pathway. Proceedings of the National Academy of Sciences of the United States of America, 2013, 110, 19336-19341.	7.1	140
255	A novel energy-oriented reconfigurable on-chip unified memory architecture based on Cache Behavior Phase Graph. , 2013, , .		1
256	Characterization of Cell Subpopulations Expressing Progenitor Cell Markers in Porcine Cardiac Valves. PLoS ONE, 2013, 8, e69667.	2.5	24
257	Bisyinshanic Acids A and B, Two Novel Diterpene Dimers from the Roots of <i>Euphorbia yinshanica</i> . Helvetica Chimica Acta, 2012, 95, 1672-1679.	1.6	24
258	Photodissociation of acryloyl chloride in the gas phase. Science China Chemistry, 2012, 55, 359-367.	8.2	4
259	Photophysical and Electronic Properties of Five PCBM-like C ₆₀ Derivatives: Spectral and Quantum Chemical View. Journal of Physical Chemistry A, 2012, 116, 255-262.	2.5	73
260	Redirecting Valvular Myofibroblasts into Dormant Fibroblasts through Light-mediated Reduction in Substrate Modulus. PLoS ONE, 2012, 7, e39969.	2.5	146
261	Dynamic Allocation of SPM Based on Time-Slotted Cache Conflict Graph for System Optimization. IEICE Transactions on Information and Systems, 2012, E95.D, 2039-2052.	0.7	0
262	Structure-Dependent All-Optical Switching in Graphene-Nanoribbon-Like Molecules: Fully Conjugated Tri(perylene bisimides). Journal of Physical Chemistry A, 2010, 114, 9130-9135.	2.5	27
263	Reaction of C2HCl2+O2: Combined TR-FTIR Spectroscopy and Electronic Structure. Chinese Journal of Chemical Physics, 2009, 22, 673-680.	1.3	0
264	Time-Resolved FTIR Study on the Reaction of CHCl2 with NO2. Chinese Journal of Chemical Physics, 2009, 22, 134-138.	1.3	0
265	Reaction Mechanisms of a Photo-Induced [1,3] Sigmatropic Rearrangement via a Nonadiabatic Pathway. Journal of Physical Chemistry A, 2009, 113, 13892-13900.	2.5	15
266	Adiabatic and Nonadiabatic Reaction Pathways of the O(³ P) with Propyne. Journal of Physical Chemistry A, 2009, 113, 23-34.	2.5	19
267	Two new diterpenes from Euphorbia kansuensis. Fìtoterapìâ, 2008, 79, 262-266.	2.2	19
268	Computational Study of the Reaction of Chlorinated Vinyl Radical with Molecular Oxygen (C2Cl3+) Tj ETQq0 0 0	rgBT /Ove 2.5	rlock 10 Tf 5

269	Three New Diterpenoids from <i>Euphorbia wallichii</i> . Chinese Journal of Chemistry, 2004, 22, 199-202.	4.9	23
-----	---	-----	----